Luminescence Spectra. The $[(Mo_6Cl_8)Cl_6]^{2-}$ ion has been shown to exhibit metal-centered luminescence near 700 nm in various solvents.[22,26] It was of great interest to see if similar emission could be detected in the $AlCl_3$–MeEtimCl melt because molten salts have rarely been used for such measurements. We found that the melt exhibits luminescence near 480 nm (uncorrected) when irradiated at wavelengths shorter than ca. 400 nm. The intensity of this luminescence could be decreased substantially, but not eliminated entirely, by treating the MeEtimCl with activated charcoal several times during the recrystallization process, suggesting that this luminescence originated from an impurity associated with the MeEtimCl. However, if solutions of $[(Mo_6Cl_8)Cl_6]^{2-}$ in 50/50 mol % melt were irradiated at exactly 400 nm, it was possible to observe an emission band centered at λ_{max} = 700 nm (uncorrected) that was very similar to that seen for this ion in nitrogen-saturated aqueous HCl (Figure 4). In addition, it was found that solutions of molybdenum(II) in the 55.0/45.0 mol % melt also luminesce at λ_{max} = 710 nm (uncorrected) (Figure 4), suggesting that the $(Mo_6Cl_8)^{2+}$ core may be preserved when molybdenum(II) is dissolved in acidic melt. However, the identity of the extant species in acidic melt could not be determined with the techniques available to us. In conclusion, these results indicate that the $AlCl_3$–MeEtimCl molten salt may be of modest value for luminescence measurements, provided that excitation of the melt or of the seemingly inescapable impurities in the melt is avoided.

Acknowledgment. This research was supported by the National Science Foundation (Grant No. CHE-8715464).

(26) Maverick, A. W.; Gray, H. B. *J. Am. Chem. Soc.* **1981**, *103*, 1298.

Contribution from the Chemistry Department and Institute for Physical Research and Technology, Iowa State University, Ames, Iowa 50011

Crystal Structures and Single-Crystal Optical Absorption Spectra for Two New Polymorphs of Tetrakis(μ-pivalato)dimolybdenum(II)[1]

Don S. Martin* and Hai-Wei Huang

Received October 25, 1989

Two new polymorphs, β- and γ-$Mo_2[O_2CC(CH_3)_3]_4$, were crystallized. The crystal structure of the β-form indicates an *I*2/*c* unit cell with *a*–*c* = 12.747 (3), 18.322 (3), and 11.369 (1) Å, β = 91.83 (1)°, and *Z* = 4. The crystal structure of the γ-form indicates a *Pbcn* unit cell with *a*–*c* = 12.711 (3), 18.351 (5), and 11.413 (3) Å and *Z* = 4. Both structures have one-dimensional chains of molecules formed by weak two Mo···O bonds between adjacent molecules, a common feature of many dimolybdenum tetracarboxylates. There is some indication of disorder of the methyl carbons in the tertiary butyl groups on the chelate rings not involved in intermolecular bonding. Single-crystal polarized absorption spectra are presented for the $1\bar{1}0$ face for the β-form and the 110 face for the γ-form. The spectra of both forms possess highly resolved vibrational structure. In the β-form the spectra indicate three different sites with origins at 21 875, 21 900, and 21 950 cm^{-1}, and in the γ-form there are two different sites with origins at 21 925 and 21 985 cm^{-1}. The spectra indicate that this first absorption band for each form is a weak nondegenerate electric dipole allowed transition with comparable intensities arising from vibronic contributions of degenerate molecular vibrations. They are therefore assigned as the $\delta \rightarrow \delta^*$ transition. There is evidence that the transition moment vectors have been shifted significantly away from the Mo–Mo bond direction. Long Frank–Condon progressions provide information about vibrational frequencies in the excited state.

Introduction

X-ray diffraction crystal structure determinations for a number of dimolybdenum tetracarboxylates[2-4] have shown that the molecules normally stack in one-dimensional chains with pairs of weak intermolecular Mo···O bonds between adjacent molecules, as is illustrated in Figure 1. The asymmetry introduced by this intermolecular bonding in the crystal packing has a profound effect on the optical absorption spectra of the crystals of these compounds.[5-7] The dimeric molecules possess an approximate local D_{4h} symmetry out through the bond to the R group in Figure 1. The first observed absorption band in the spectra is considered to correspond to the spin-allowed $\delta \rightarrow \delta^*$ transition, ($^1A_{1g} \rightarrow {}^1A_{2u}$; $b_{2g} \rightarrow b_{1u}$). Such a molecular transition is electric dipole allowed with *z* polarization, i.e., with the transition moment directed along the metal–metal bond, which is the 4-fold symmetry axis. The transitions are weak, however, presumably because their intensity is dependent upon the small interatomic overlap of the δ orbitals on the separate metal atoms. The spectra for these compounds have rich vibrational structure; long Franck–Condon progressions, based on the Mo–Mo stretching frequency, have been observed on a number of vibronic origins as well as the O–O line. The polarization ratio for the O–O line in the acetate for two different faces[5] indicated that the transition-moment vector for the $\delta \rightarrow \delta^*$ transition did not lie along the metal–metal bond but was oriented 32° away from the bond and was approximately in the plane containing the intermolecular Mo···O bonds. Polarization ratios for other carboxylates have also indicated an appreciable deviation of the transition moment vectors away from the metal–metal bond.

Very recently, Cotton and Zhong[8] reported the spectra for $Mo_2[O_2CC(C_6H_5)_3]_4 \cdot 3CH_2Cl_2$. This crystal has a tetragonal lattice with the metal–metal bond aligned with the crystallographic *c* axis, and there was no intermolecular bonding. The spectra indicated multiple sites that were dependent on the loss of CH_2Cl_2 molecules. However, origin lines were *c* and therefore *z* polarized while a number of vibronically excited lines had *a* and therefore *x*,*y* polarization. These results together with the pattern of hot bands observed are also consistent with an assignment of the first absorption band as a weak electric dipole allowed $\delta \rightarrow \delta^*$ transition.

Cotton et al.[9] reported the preparation and structure for a triclinic crystal of tetrakis(μ-pivalato)dimolybdenum(II) which

(1) From the dissertation of H.-W.H. submitted in partial fulfillment of the Ph.D. degree, 1985.
(2) Cotton, F. A.; Norman, J. G.; Stults, B. R.; Webb, T. R. *J. Coord. Chem.* **1976**, *5*, 217.
(3) Cotton, F. A.; Mester, Z. C.; Webb, T. R. *Acta Crystallogr., Sect. B* **1974**, *30*, 2768.
(4) Cotton, F. A.; Norman, J. G. *J. Coord. Chem.* **1971**, *1*, 161.
(5) Martin, D. S.; Newman, R. A.; Fanwick, P. E. *Inorg. Chem.* **1979**, *18*, 2511.
(6) Martin, D. S.; Newman, R. A.; Fanwick, P. E. *Inorg. Chem.* **1982**, *21*, 3400.
(7) Robbins, G. A.; Martin, D. S. *Inorg. Chem.* **1984**, *23*, 2086.
(8) Cotton, F. A.; Zhong, B. *J. Am. Chem. Soc.* **1990**, *112*, 2256.
(9) Cotton, F. A.; Extine, M.; Gage, L. D. *Inorg. Chem.* **1978**, *17*, 172.

0020-1669/90/1329-3674$02.50/0

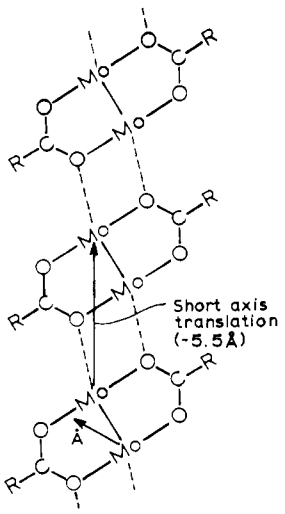

Figure 1. Arrangement of intermolecular bonding common for most crystals of dimolybdenum tetracarboxylates. Two carboxylate rings in each molecule were omitted for clarity.

did not contain the normal stacking chains of the other carboxylates that have been studied. There were stacking chains in this structure with the pairs of Mo···O intermolecular bonds. However, the intermolecular bonding involved *cis*-Mo_2O_2C rings on each molecule rather than the trans rings shown in Figure 1. Since it was of interest to determine changes in the crystal spectra that might be a consequence of this different structural feature, we prepared samples of this compound for spectroscopic studies. Among our preparations were a number of thin needles suitable for spectroscopic studies. An examination of these needles revealed that there were two frequently occurring types of faces with different optical features. An X-ray diffraction examination of the crystals with the different types of faces revealed that neither possessed the structure of Cotton et al. but that they were two new polymorphic forms, one with a monoclinic structure and the other with an orthorhombic form. The present work is concerned with the structures and spectra of these two polymorphic forms.

Experimental Section

Preparations. $Mo_2(O_2CC(CH_3)_3)_4$ was prepared by reacting $Mo(CO)_6$ with pivalic acid in refluxing *o*-dichlorobenzene under N_2 for three days according to the procedure of McCarley et al.[10] The compound crystallized as slender yellow crystals when the reaction mixture was cooled to room temperature. A number of crystals were ideally suited for spectroscopy. The crystalline product was filtered out, washed with benzene and cyclohexane, and dried under vacuum for 1 day. The procedure differed from that used by Cotton et al.[9] in that they sublimed a small amount of similarly prepared material under vacuum in a sealed glass tube.

An examination of the crystals under a polarizing microscope clearly indicated two types of faces on thin needles. For one type of face the extinctions between crossed polarizers occurred about 18° off the needle axis. Furthermore, the extinctions were not sharp under white light but passed from a distinct dark blue to a dark red color as the extinction was passed. Such behavior indicated that the extinction direction is rather strongly wavelength dependent. For the other type of face the extinctions were sharp and were aligned parallel with and perpendicular to the needle edges. Accordingly, crystals with each type of face were mounted for X-ray diffraction in order to confirm the cell parameters for the structure of Cotton et al. and to identify the faces. Instead of confirmation of Cotton's triclinic axes, the crystals each yielded a different set of axes, indicating two new polymorphic forms. The crystals with extinctions off the needle axis possessed monoclinic axes and have been designated as the β-form with Cotton's triclinic structure assigned the α-form. The crystals with sharp extinctions along the needle edges proved to have orthorhombic axes and have been designated as the γ-form.

Spectroscopic Measurements. The equipment and procedures for recording the polarized optical spectra have been described previously.[11,12]

(10) McCarley, R. E.; Templeton, J. L.; Colburn, T. J.; Katovic, V.; Hoxmeier, R. J. *Adv. Chem. Ser.* **1976**, *No. 150*, 318.
(11) Martin, D. S. *Inorg. Chim. Acta Rev.* **1971**, *5*, 107.

Table I. Crystallographic Parameters for the $Mo_2[O_2CC(CH_3)_3]_4$ Polymorphs

	α-Mo_2-$[O_2CC(CH_3)_3]_4$[a]	β-Mo_2-$[O_2CC(CH_3)_3]_4$	γ-Mo_2-$[O_2CC(CH_3)_3]_4$
space group	$P\bar{1}$	$I2/c$	$Pbcn$
cryst system	triclinic	monoclinic	orthorhombic
a, Å	11.793 (3)	12.747 (3)	12.711 (3)
b, Å	12.154 (4)	18.322 (3)	18.351 (5)
c, Å	10.403 (4)	11.369 (1)	11.413 (3)
α, deg	90.07 (3)	90.0	90.0
β, deg	104.61 (3)	91.83 (1)	90.0
γ, deg	71.33 (2)	90.0	90.0
V, Å^3	1361.8 (7)	2654.1 (8)	2662 (1)
Z	2	4	4
V/Z, Å^3	680.9 (4)	663.5 (2)	665.5 (3)
R	0.060	0.055	0.057
R_w	0.085	0.084	0.084
site sym	1	$\bar{1}$	$\bar{1}$

[a] Reference 9.

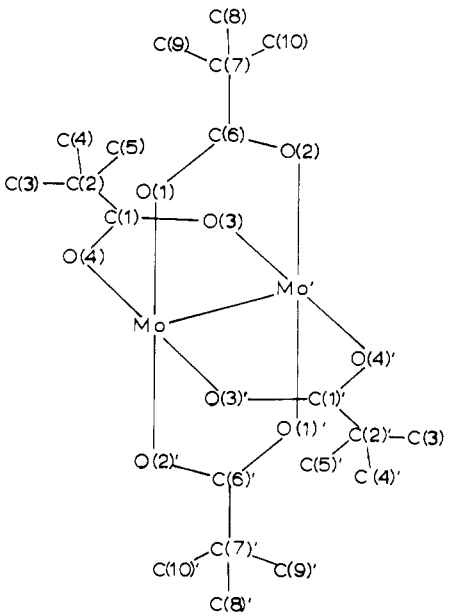

Figure 2. Atom-labeling system used in the structure of β- and γ-$Mo_2[O_2CC(CH_3)_3]_4$.

The spectra with well-resolved vibrational features were recorded with slit settings that provided a dispersion of no more than 0.12 nm. Plots for the highly resolved spectra were recorded from digital output each 0.1 nm with a scan speed of 0.05 nm/s.

X-ray Diffraction Methods. Methods for collecting X-ray diffraction data and for identifying faces and axial directions in single crystals have been described previously.[7] The crystallographic lattice parameters for the β- and the γ-$Mo_2[O_2CC(CH_3)_3]_4$ are collected in Table I.

β-$Mo_2[O_2CC(CH_3)_3]_4$ (Monoclinic). A 1.0 × 0.09 × 0.05 mm crystal for which the largest face possessed an extinction 18° off the needle edge was cemented to a glass fiber and mounted on the X-ray diffraction so that the axes could be compared with those of Cotton et al.'s triclinic form. When the *b*-axis oscillation photographs exhibited a mirror plane, and a set of monoclinic axes were indicated, a full set of diffraction data were collected that totaled 10759 reflections of which 1948 independent reflections, having $|F_o| > 3\sigma(F_o)$, were used for a structure solution. The program LATT[13] used $\pm 2\theta$ values for 20 reflections to refine the cell parameters reported in Table I. The monoclinic space group assignment $I2/c$ was based on the systematic extinctions of $h + k + l$ odd for the hkl reflections, of l odd for the $h0l$ reflection, and of k odd for the $0k0$ reflections. Initial Mo atom positions were obtained from a three-dimensional Patterson map. A subsequent electron-density map yielded the positions of the remaining non-hydrogen atoms. Positional parame-

(12) Fanwick, P. E.; Martin, D. S.; Webb, T. R.; Robbins, G. A.; Newman, R. A. *Inorg. Chem.* **1978**, *17*, 2723.
(13) Jacobson, R. A. An Algorithm for Automatic Indexing and Bravais Lattice Selection: The Programs BLIND and ALICE. Ames Laboratory USAEC Report IS-3469; Iowa State University: Ames, Iowa, 1974.

Table II. Fractional Positional Parameters for the β- and γ-Tetrakis(μ-pivalato)dimolybdenum(II)

	x	y	z
	β-$Mo_2[O_2CC(CH_3)_3]_4$ (Monoclinic)		
Mo	0.53843 (3)	0.49597 (3)	0.42058 (4)
O(1)	0.5224 (4)	0.3823 (3)	0.4180 (4)
O(2)	0.4409 (4)	0.3904 (3)	0.5867 (4)
O(3)	0.3143 (4)	0.5108 (2)	0.4903 (4)
O(4)	0.3943 (3)	0.5021 (2)	0.3199 (4)
C(1)	0.3112 (5)	0.5072 (3)	0.3802 (6)
C(2)	0.2055 (5)	0.5073 (3)	0.3141 (6)
C(3)	0.1940 (6)	0.4353 (4)	0.2431 (7)
C(4)	0.2014 (6)	0.5736 (4)	0.2297 (7)
C(5)	0.1167 (6)	0.5132 (5)	0.4012 (8)
C(6)	0.4731 (6)	0.3534 (4)	0.5000 (6)
C(7)	0.452 (1)	0.2734 (5)	0.499 (1)
C(8)	0.545 (1)	0.230 (1)	0.480 (1)
C(9)	0.367 (2)	0.265 (1)	0.387 (2)
C(10)	0.375 (1)	0.2521 (9)	0.592 (2)
	γ-$Mo_2[O_2CC(CH_3)_3]_4$ (Orthorhombic)		
Mo	0.46070 (5)	0.50439 (3)	0.42005 (6)
O(1)	0.4745 (4)	0.6182 (3)	0.4199 (6)
O(2)	0.5592 (4)	0.6091 (3)	0.5899 (6)
O(3)	0.6862 (4)	0.4902 (3)	0.4945 (5)
O(4)	0.6050 (4)	0.4998 (3)	0.3236 (5)
C(1)	0.6888 (6)	0.4949 (4)	0.3844 (8)
C(2)	0.7934 (7)	0.4951 (5)	0.3220 (8)
C(3)	0.8039 (7)	0.5659 (5)	0.250 (1)
C(4)	0.7981 (7)	0.4273 (6)	0.240 (1)
C(5)	0.8828 (8)	0.4897 (7)	0.4118 (9)
C(6)	0.5236 (6)	0.6469 (5)	0.5046 (9)
C(7)	0.548 (1)	0.7267 (7)	0.501 (1)
C(8)	0.459 (2)	0.772 (1)	0.479 (2)
C(9)	0.634 (2)	0.733 (1)	0.394 (2)
C(10)	0.620 (2)	0.749 (1)	0.599 (2)

ters were refined first by block-diagonal matrices and finally by full-marix least squares. Since in both the monoclinic and orthorhombic forms the molecules possess an inversion symmetry, a common system for the labeling of atoms could be used, which is illustrated in Figure 2. Thermal parameters for three of the six independent methyl carbons could not be refined anisotropically, and only isotropic parameters were obtained. Atomic positions are presented in Table II. Temperature factors were included with the supplementary material. Details of the structure are discussed in the comparison of the β- and the γ-polymorphs.

γ-$Mo_2[O_2CC(CH_3)_3]_4$ (Orthorhombic). A 0.32 × 0.14 × 0.08 mm crystal for which the largest face possessed sharp extinctions aligned with and perpendicular to the crystal edge was mounted for axial determinations. The transformation matrices provided a set of orthogonal axes, and the oscillation photographs for all three of these axes exhibited the mirror planes required for an orthorhombic system. A total of 6118 reflections were collected of which 1607 independent reflections, having $|F_o| > 3\sigma(F_o)$, were used in the structure solution. The cell parameters, given in Table I, were based on ±2θ values of 15 reflections. The assignment of the space group as *Pbcn* was based on the systematic extinctions of *k* odd for the 0*kl* reflection, of *l* odd for the *h*0*l* reflections, of $h + k$ odd for the *hk*0 reflections, of *h* odd for the *h*00 reflections, and of *k* odd for the 0*k*0 reflections. The structure determination followed that of the β-polymorph by means of the Patterson map, the electron-density map, the block-diagonal matrices, and finally the full-matrix least squares. As with the β-polymorph, only isotropic thermal parameters could be refined for three of the six independent methyl carbons. The atomic positions for this structure are also presented in Table II.

Results and Discussion

Comparison of the Structures for Tetrakis(μ-pivalato)dimolybdenum(II). The non-hydrogen bond lengths and the bond angles for the β- and γ-polymorphs are listed in Table III. For the intramolecular distances and angles the agreement between *each structure* is within the uncertainty indicated for the values. With perhaps one exception, noted below, they are in extraordinary agreement with the values reported for the α-form as well.[9]

In each structure there are the one-dimensional chains that have characterized the majority of the dimolybdenum tetracarboxylates. In both the β- and γ-polymorphs the Mo′ atom approaches sufficiently close to form a weak bond to O(4) on a neighboring molecule, while the O(4)′ forms an equivalent bond to the Mo

Table III. Interatomic Distances and Angles with Standard Deviations for the β- and γ-Tetrakis(μ-pivalato)dimolybdenum(II)

	β-$Mo_2[OCC(CH_3)_3]_4$ (*I*2/*c*)	γ-$Mo_2[O_2CC(CH_3)_3]_4$ (*Pbcn*)
	Distances (Å)	
Mo–Mo′	2.087 (1)	2.087 (1)
Mo–O(1)	2.092 (5)	2.095 (6)
Mo–O(2)′	2.100 (5)	2.101 (6)
Mo–O(3)′	2.107 (5)	2.109 (5)
Mo–O(4)	2.136 (5)	2.141 (5)
Mo–O(4)(ax)	2.894 (5)	2.905 (5)
O(1)–C(6)	1.257 (9)	1.27 (1)
O(2)–C(6)	1.276 (9)	1.28 (1)
O(3)–C(1)	1.254 (8)	1.26 (1)
O(4)–C(1)	1.283 (8)	1.28 (1)
C(1)–C(2)	1.52 (1)	1.51 (1)
C(2)–C(3)	1.55 (1)	1.54 (1)
C(2)–C(4)	1.55 (1)	1.56 (1)
C(2)–C(5)	1.53 (1)	1.53 (1)
C(6)–C(7)	1.49 (1)	1.50 (1)
C(7)–C(8)	1.45 (2)	1.43 (3)
C(7)–C(9)	1.65 (2)	1.65 (3)
C(7)–C(10)	1.52 (2)	1.50 (3)
	Angles (deg)	
Mo′–Mo–O(1)	92.0 (1)	92.2 (2)
Mo–Mo′–O(2)	91.5 (1)	91.6 (2)
Mo–Mo′–O(3)	91.4 (1)	91.3 (2)
Mo′–Mo–O(4)	92.3 (1)	92.1 (2)
Mo–Mo′–O(4)(ax)	167.5 (1)	166.6 (1)
O(1)–Mo–O(4)	87.87 (9)	88.1 (1)
O(1)′–Mo′–O(3)	91.90 (8)	91.6 (1)
O(2)–Mo′–O(3)	88.07 (8)	88.0 (1)
O(2)′–Mo–O(4)	91.92 (8)	92.1 (1)
Mo–O(1)–C(6)	117.4 (3)	117.1 (4)
Mo′–O(2)–C(6)	116.9 (3)	117.0 (4)
Mo′–O(3)–C(1)	118.4 (3)	118.8 (4)
Mo–O(4)–C(1)	115.3 (3)	116.0 (3)
Mo–O(4)–Mo(ax)	103.21 (7)	104.17 (9)
O(3)–C(1)–O(4)	122.5 (6)	121.7 (7)
O(1)–C(6)–O(2)	122.0 (7)	122.0 (9)
O(3)–C(1)–C(2)	119.5 (5)	119.6 (7)
O(4)–C(1)–C(2)	118.0 (5)	118.7 (6)
O(1)–C(6)–C(7)	120.2 (7)	119.2 (8)
O(2)–C(6)–C(7)	117.8 (6)	118.6 (8)
C(1)–C(2)–C(3)	108.8 (4)	109.3 (7)
C(1)–C(2)–C(4)	108.6 (4)	108.4 (5)
C(1)–C(2)–C(5)	110.0 (4)	109.7 (5)
C(3)–C(2)–C(4)	110.1 (6)	110.4 (8)
C(3)–C(2)–C(5)	109.7 (6)	110.3 (8)
C(4)–C(2)–C(5)	109.5 (6)	108.7 (8)
C(6)–C(7)–C(8)	113.1 (8)	114 (1)
C(6)–C(7)–C(9)	102.2 (6)	103.1 (7)
C(6)–C(7)–C(10)	111.6 (7)	97.4 (7)
C(8)–C(7)–C(9)	111 (1)	110 (1)
C(8)–C(7)–C(10)	121 (1)	117 (1)
C(9)–C(7)–C(10)	95 (1)	97 (1)

on the same neighbor. Thus, there are pairs of weak bonds, equivalent by symmetry, between adjacent neighbors. There is a pair of equivalent bonds involving Mo and O(4) on the other side of the molecule. Therefore, the O(4) and O(4)′ atoms have an environment considerably different from that of other O's. The Mo–O(4) bond is 0.035 and 0.038 Å longer than the average of the other Mo–O bonds in the β- and γ-forms, respectively. In the α-form the intermolecular bonding as through cis rather than through the trans rings and the two Mo–O bonds were 2.126 (5) and 2.135 (5) Å compared to 2.135 (5) and 2.141 (5) Å for the β- and γ-forms.

The carbon atoms, being the lightest of the non-hydrogens, are given least precisely by the X-ray diffraction. The isotropic temperature factors for C(8), C(9), and C(10), the methyl carbons on the rings not involved in intermolecular bonding, as well as some of the factors for C(7) were significantly larger than factors for other carbons. This feature together with large deviations from expected C–C single-bond distances and the tetrahedral angles about C(7) imply that there may be considerable disorder in the

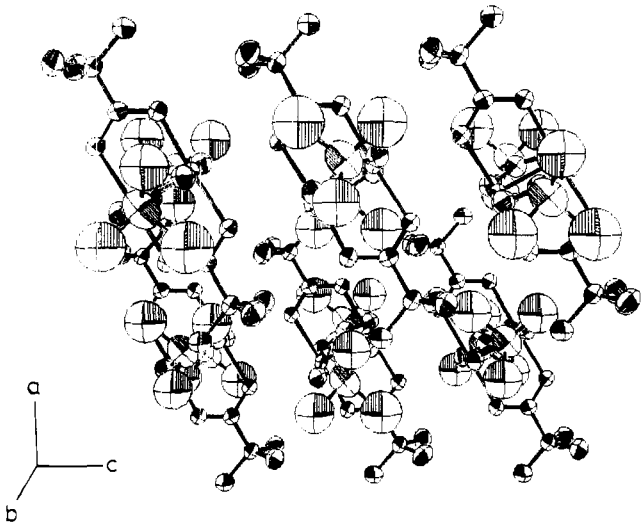

Figure 3. Molecular struture and packing in chains for β-$Mo_2[O_2CC(CH_3)_3]_4$ (monoclinic).

tertiary butyl groups attached to those chelate rings not involved in intermolecular bonding. These groups might be expected to have less rigidly established positions. A similar trend can be seen in the α-structure where, however, only isotropic thermal parameters were refined for all the carbons. Despite these indications of disorder, the R values of 0.055 and 0.057 and R_w values of 0.084 and 0.084 are about as low as can be expected for such X-ray structure determinations.

Whereas the Mo–O bonds in the chelate rings fall in the range 2.09–2.14 Å, the intermolecular or Mo′–O(4) axial bonds are much weaker and have bond lengths of 2.894 (5) and 2.905 (5) Å in the β and γ-structures, respectively. These are comparable to the two intermolecular bonds of 2.870 (5) and 2.926 (5) Å found in the α-form. The optimum axial bond for Mo is expected to be colinear with or at 180° to the Mo–Mo′ bond. However, the optimum Mo–O (4)–Mo′ axial bond would be 120°, using the sp^2 hybrid orbital for the oxygen. These two optimum conditions are incompatible, and the compromise involves Mo–Mo′–O(4) axial angles of 167.5 (1) and 166.6 (1)°, about 13° off the 180° optimum. The Mo–O(4)–Mo′ axial angles are only 103.21 (7) and 104.17 (9)°, averaging about 16° away from the 120° optimum. The pairs of bonds between the two molecules are approximately but not exactly parallel.

The one-dimensional chains, which run through the crystal in the c direction, can be considered to be rodlike entities. These rods have approximately a close-packed structure in that each rod has six neighboring rods packed around it. ORTEP views for the two structures are presented in Figures 3 and 4. Each view shows three members of two chains that pass through a unit cell, one somewhat behind the other. As is evident for the figures, the monoclinic structure has a roughly parallel alignment of the molecules in the two chains whereas the orthorhombic structure possesses a "herring bone" alignment of the molecules. The parallel alignment provides a slightly more efficient packing, since its molecular volume, tabulated in Table I, is 2 $Å^3$ smaller than that for the orthorhombic. Both are more efficiently packed than the α-form, which has a molecular volume some 15 $Å^3$ larger than the orthorhombic form. The large temperature factors for some of the methyl carbons are clearly evident from the ORTEP drawings in Figures 3 and 4.

Single-Crystal Spectra. β-$Mo_2[O_2CC(CH_3)_3]_4$. The spectroscopic face of the crystals was identified as $1\bar{1}0$. The molecules were stacked in the one-dimensional chains along the c axis, which was also the needle axis of the crystals. The extinction directions, observed with the polarizing microscope, were at 18° (to the right of the c axis) and at −72°. However, the microscopic observation indicated a distinct wavelength dependence of the extinction direction. Our experience with the tetrakis(μ-acetato)dimolybdenum(II) crystals showed that with a wavelength dependence of the extinctions, the polarizer angle cannot be safely set

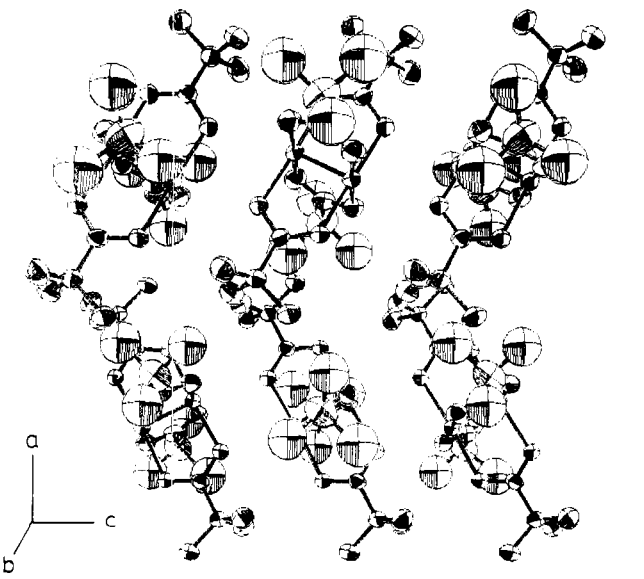

Figure 4. Molecular struture and packing in chains for γ-$Mo_2[O_2CC(CH_3)_3]_4$ (orthorhombic).

at the angles observed in the polarizing microscope.

For the crystals of both polymorphs the first absorption band at 300 K has a maximum at ca. 23 000 cm^{-1}. At 6 K this band for the monoclinic crystals develops a rich vibrational structure. Extended plots of the low-energy region of this band recorded for the $1\bar{1}0$ face at polarizer settings of 18 and −72° are presented in Figure 5. When the plane of polarized light entering a crystal is rotated, the observed absorbance will be a maximum or minimum at the extinction angles. Crystal spectra were recorded for steps of 10° in the polarized angle. The 18 and the −72° curves shown in Figure 5 had the minimum and maximum values for the lines labeled A in the figure. This, for these lines the indicated extinctions within the experimental uncertainty coincided with the optical extinctions assigned from the polarizing microscope. Wavenumbers of resolvable peaks and shoulders have been recorded, and the assignments of progression lines have been included in Table IV.

The peaks in the crystal spectra of Figure 5 were quite sharp, and insofar as they could be resolved, every absorption feature occurred as three lines; e.g., there were three A_0 lines (A_0^1, A_0^2, A_0^3). Extended Franck–Condon progressions based on each of these three origins could be identified. The first member, A_0^1, is quite weak. At 25 cm^{-1} higher energy A_0^2 is considerably stronger, and at 50 cm^{-1} higher still A_0^3 has an intensity comparable to that of A_0^2. The polarization ratio, $I(-72°)/I(18°)$, is 2.8 and the A progressions dominate the −72° spectrum. In the 18° spectrum triple B–E progressions are evident. The labeling of these progressions follow generally our assignments for other dimolybdenum tetracarboxylate spectra.[5-7] The intensities of the B, C, and E lines did not change greatly as the polarizer was rotated, and it can be seen from Figure 5 that they have approximately equal intensities in the 18 and −72° polarizations. The D lines in the −72° polarization were masked somewhat by the high-intensity A lines.

The possibility that Davydov splitting might account for the multiple lines in the spectra was considered. A treatment of the Davydov states and their transition moments has been presented in the Appendix. First of all, a primitive cell for the $I2/c$ space group contains only two symmetry-related molecules so there can be only two Davydov states and a third line could not be explained. Furthermore, because of the nearly parallel orientation of the two molecules, one of the transition moments will be much larger than the other. For a z-polarized transition, the transition moment ratio squared, $(\mu_I/\mu_{II})^2$, is about 200. In addition, a much different polarization ratio for the two Davydov transitions would be expected.

It has therefore been concluded that the presence of three lines, two about equally strong and one weaker and each with the same

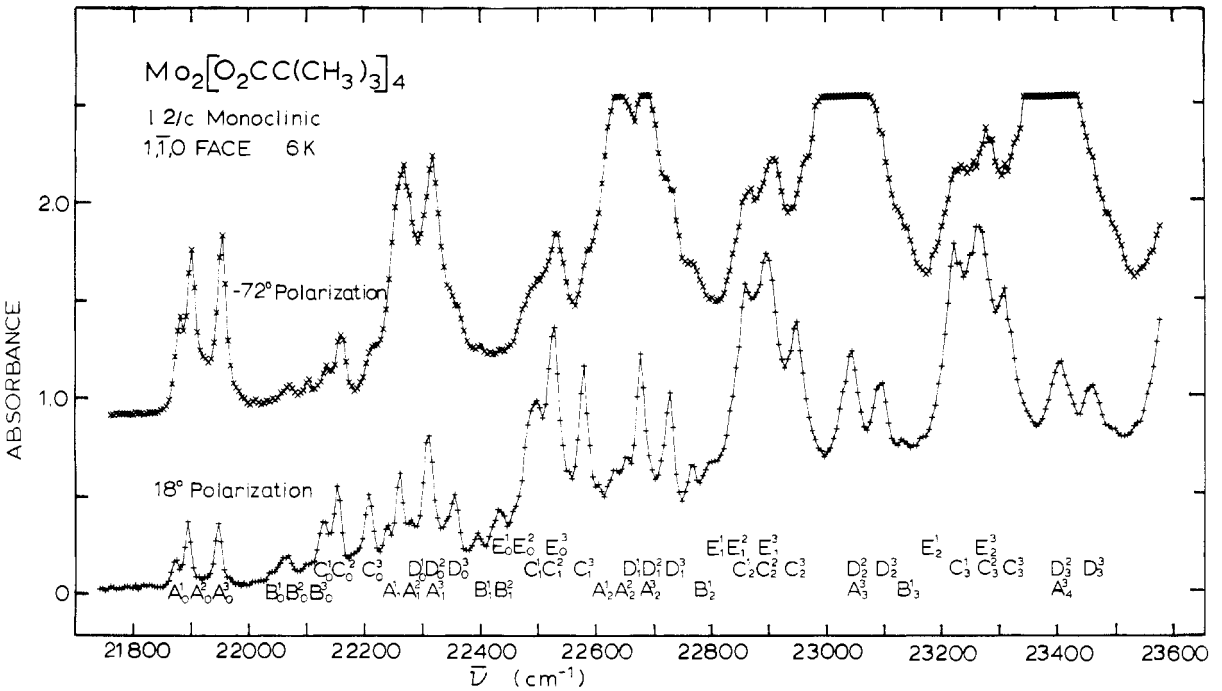

Figure 5. Low-temperature polarized spectra for the $1\bar{1}0$ face of a β-$Mo_2[O_2CC(CH_3)_3]_4$ (monoclinic) crystal, 52 ± 10 μm thick.

Table IV. Vibrational Details in the Low-Energy Absorption Band of β-Tetrakis(μ-pivalato)dimolybdenum(II) (Monoclinic) at 6 K

assgnt	ν, cm^{-1}	$\Delta\nu$,[a] cm^{-1}	assgnt	ν, cm^{-1}	$\Delta\nu$,[a] cm^{-1}
A_0^1	21 875		A_2^1	22 600	360
A_0^2	21 900	(25)	A_2^2	22 630	370
A_0^3	21 950	(75)	D_1^1	22 650	370
B_0^1	22 040	(165)	A_2^3, D_1^2	22 675	365
B_0^2	22 070	(195)	D_1^3	22 275	365
B_0^3	22 115	(240)	B_2^1	22 760	365
C_0^1	22 130	(255)	E_1^1	22 800	370
C_0^2	22 150	(275)	E_1^2	22 830	370
C_0^3	22 210	(335)	C_2^1	22 860	360
A_1^1	22 240	365	C_2^2, E_1^3	22 890	365
A_1^2	22 260	360	C_2^3	22 945	365
D_0^1	22 280	(405)	A_3^3, D_2^2	23 040	365
A_1^3, D_0^2	22 310	360, (435)	D_2^3	23 090	365
D_0^3	22 360	(485)	B_3^1	23 130	370
B_1^1	22 400	360	E_2^1	23 160	360
E_0^1	22 430	(555)	C_3^1	23 220	360
E_0^2	22 460	(585)	C_3^2, E_2^3	23 260	370
C_1^1	22 500	370	C_3^3	23 305	360
C_1^2, E_0^3	22 525	375, (650)	A_4^3, D_3^2	23 400	360
C_1^3	22 580	370	D_3^3	23 455	365

[a] Values in parentheses give the difference, $\Delta\bar{\nu}$, from the A_0^1 line. Values without parentheses give the $\Delta\bar{\nu}$ values from the preceding line in a progression.

Table V. Vibrational Details in the Low-Energy Absorption Band of γ-Tetrakis(μ-pivalalto)dimolybdenum(II) (Orthorhombic) at 6 K

assgnt	ν, cm^{-1}	$\Delta\nu$,[a] cm^{-1}	assgnt	ν, cm^{-1}	$\Delta\nu$,[a] cm^{-1}
A_0^1	21 925		A_2^2	22 720	370
A_0^2	21 985	(60)	D_1^2	22 765	375
B_0^1	22 100	(175)	B_2^1	22 845	375
C_0^1	22 185	(260)	E_1^1	22 885	375
C_0^2	22 245	(320)	C_2^1	22 930	375
A_1^1	22 290	365	C_2^2	22 990	375
D_0^1	22 330	(405)	A_3^1	23 030	370
A_1^2	22 350	(425)	D_2^1	23 075	370
D_0^2	22 390	(465)	A_3^2	23 100	380
B_1^1	22 470	370	D_2^2	23 130	365
E_0^1	22 510	(585)	B_3^1	23 210	365
C_1^1	22 555	370	E_2^1	23 250	365
C_1^2	22 615	370	C_3^1	23 290	360
A_2^1	22 660	370	A_4^1	23 390	360
D_1^1	22 705	375	D_3^1	23 440	365

[a] Values in parentheses give the difference, $\Delta\bar{\nu}$, from the A_0^1 line. Values without parentheses give the difference $\Delta\bar{\nu}$ from the preceding line in the progression.

polarization ratio, must be due to two major sites in the crystal and one minor site that gives the lowest energy transition. Since the crystal structure has only one site type, it therefore is not consistent with the spectra. The X-ray diffraction was performed at room temperature. The line splittings disappear about 80 K at which point there is extensive thermal broadening. It is possible that there is a second-order phase transition between 80 and 300 K that reduces the symmetry. However, it seems more likely that since the structure determination implied some disorder in the location of the methyl carbons in the tertiary butyl groups, the site differences are caused by this sort of disorder. The details of the spectra in Figure 5 have been duplicated for several crystals whose spectra were recorded, and the presence of two major peaks and one minor peak have been consistently reproduced in the preparations. Site differences have also appeared in crystal spectra of polymorphs of tetrakis(μ-formato)dimolybdenum(II) and tetrakis(μ-trifluoroacetato)dimolybdenum(II). Recently, some have been reported for tetrakis(μ-triphenylacetato)dimolybdenum(II), where the site differences were shown to result from differing amounts of CH_2Cl_2 that were included in the crystal.[8]

It has been concluded that the A_0 lines are the 0–0 transitions of the $\delta \rightarrow \delta^*$ electronic transition for the different sites. This transition in D_{4h} symmetry is electric dipole allowed in z polarization, and the B_0, C_0, D_0, and E_0 origins are vibronically enabled in x,y polarization by means of E_g molecular vibrations.

For two extinction direction vectors, **Ex1** and **Ex2**, the polarization ratio, I_1/I_2, has been calculated by the expression

$$\frac{I_1}{I_2} = \frac{\sum_i \cos^2 \theta_{1,i}}{\sum_i \cos^2 \theta_{2,i}} \qquad (1)$$

where $\theta_{1,i}$ is the angle between the transition moment of the ith molecule and the **Ex1** extinction vector, etc. and the sum is over the symmetry-equivalent molecules in a primative cell. For a transition moment aligned with the molecular z axis or the metal–metal bond, as would be required with a strict D_{4h} symmetry, the calculated polarization ratio, $I(-72°)/I(1,8)$, was 0.49, in very poor agreement with the experimental value of 2.8. In the acetate crystals it was shown that the transition moment lay

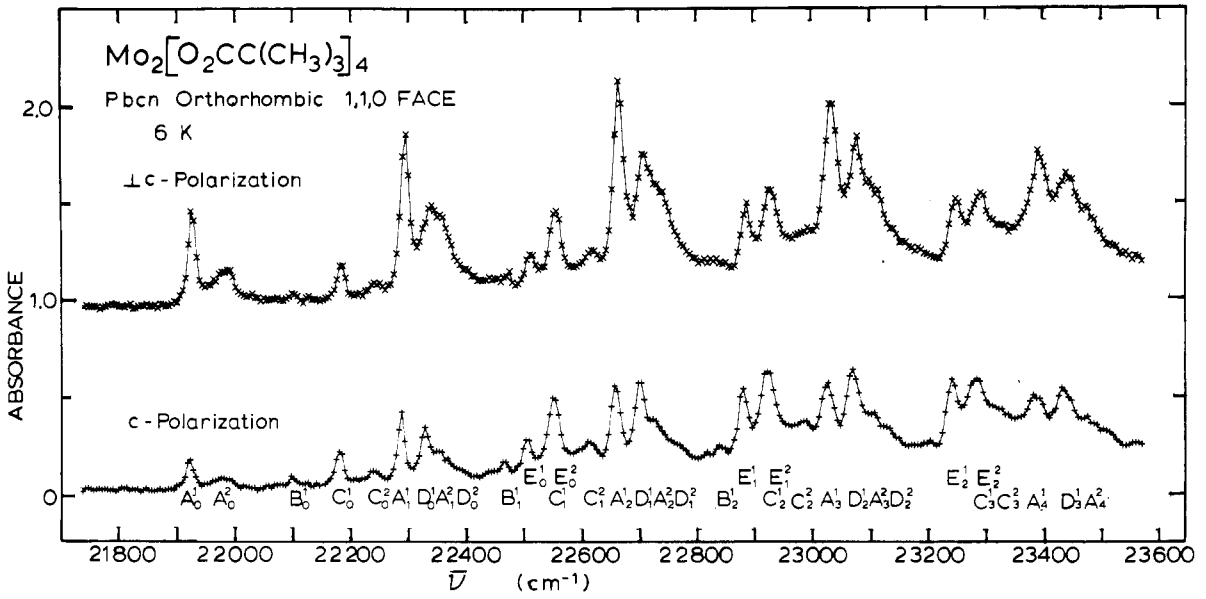

Figure 6. Low-temperature polarized spectra for the 110 face of a γ-$Mo_2[O_2CC(CH_3)_3]_4$ (orthorhombic) crystal, 20 ± 10 μm thick.

approximately in the plane defined by Mo, Mo′, and O(4) and that it was shifted away from the Mo–Mo′ bond toward O(4) by 32°. In the present case a calculated polarization ratio was obtained with a similar shift of the transition moment by 29°. This angle may be compared with shifts of 34° for tetrakis(μ-trifluoroacetato)dimolybdenum(II) and 39° for the α- and the β-tetrakis(μ-formato)dimolybdenum(II), which would be consistent with the observed polarization ratios.

The separation of the lines in the Franck–Condon progressions is by 365 (5) cm^{-1}, which represent the A_{1g} metal–metal stretching frequency in the excited state and which is consistent with that of the other carboxylates. The B–E progressions are assigned as vibronically excited by E_g vibrations. The B and E progressions are the most intense, and their frequencies in the excited electronic state are obtained by the heights of their origin above the A origin. These indicate frequencies of 255 cm^{-1} for B and 563 cm^{-1} for E. These values can be compared to the 380 and 780 cm^{-1} observed for the formate. However, for all the compounds with acetate and substituted acetate, i.e., $O_2CCH_3^-$, $O_2CCF_3^-$, $O_2CCPh_3^-$, and $O_2C(CH_3)_3^-$, there have been intense progressions based on vibrations in the ranges 239–275 and 495–563 cm^{-1}. In a number of instances but not in the formate there are one or two progressions with origins below C as in the present case with B at 175 cm^{-1}. Also a progression with origins between C and E as in this case with D is evident but not in the formate or trifluoroacetate.

γ-$Mo_2[O_2CC(CH_3)_3]_4$. The low-temperature spectra for the low-energy region of the 23 000-cm^{-1} band for the 110 face of the γ-polymorph are presented in Figure 6. The *c* axis lies in this face, which for an orthorhombic crystal will be one of the extinction directions. The other extinction direction has been designated as $\perp c$. Some differences from the spectra of the monoclinic crystals are immediately evident. Here, there are two components for each feature in the spectra. First, there is a relatively sharp peak and about 60 cm^{-1} higher is a much lower broader peak. Despite the disparity in heights the integrated intensities of the two peaks are comparable; the higher peak was estimated to have only 30% higher intensity than the shorter. Again, the presence of two peaks can not be attributed to Davydov states. According to the treatment in the Appendix, there are four Davydov states. However, transition to one of the states in *Pbcn* is forbidden. For the 110 face, one transition would be allowed for *c* polarization, and two other transitions would be allowed in $\perp c$ polarization. Hence, again, the splitting of lines observed can most likely be attributed to site differences that are not predicted from the crystal structure. It is interesting that the splitting patterns of the two polymorphs are so different. The energies of the lines for the A–E, together with the Franck–Condon separations, are given in Table V.

The polarization ratio for the A lines is $I(\perp c)/I(c) = 2.7$. B–E lines had comparable intensities in the two polarizations. Again, it is logical to assign the A_0 lines as origins of a $\delta \rightarrow \delta^*$ transition and the B_0, C_0, D_0, and E_0 lines as origins excited by four E_g vibration sets in the local D_{4h} symmetry. If the transition moment for the A lines were directed along the metal–metal bond, then the polarization ratio was calculated to be $I(\perp c)/I(c) = 0.15$. Here again, there is disagreement between the observed polarization ratio and that calculated for a strictly *z*-polarized transition. In this case it was found that a transition moment vector lying in the Mo–Mo–O(4) plane would need to be shifted 40° off the metal–metal bond toward O(4) to produce the observed polarization ratio for the A lines.

The average separation of the Franck–Condon progressions is 370 (5) cm^{-1}, and the energies of the B–E vibrations in the excited state, indicated by the difference between their origins and the A origin, amount to 175, 260, 405, and 585 cm^{-1}, respectively. Hence, the vibrational pattern for the bands in the two isomers are quite similar, and there is an overlap of the ranges of the transition origins of the different sites as well. Spectra are now available for eight different crystals of the dimolybdenum(II) tetracarboxylates, and the origins have all been in the narrow range 21 700–22 080 cm^{-1}.

Conclusions

The two new polymorphs reported here, in contrast to the α-polymorph, contain the one-dimensional chains formed by weak intermolecular twin bonds involving trans-chelate rings that have occurred in the majority for this class of compounds that have been reported. As is the usual case with this type of structure, the intermolecular bonding comprises the molecular symmetry so that observed polarization ratios deviate greatly from those calculated by a simple oriented molecule model. Both polymorphs show evidence of major site differences that are not consistent with the crystal structure and that have now been observed in several instances. With the collection of spectra for a number of these compounds with highly resolved vibrational structure at low temperatures, it has now been possible to characterize this low-energy band in their spectra as a weak electric dipole allowed transition with considerable intensity contribution from vibronic excitation. There seems little doubt, especially in view of the recent work by Cotton and Zhong,[8] but that this is the $\delta \rightarrow \delta^*$ transition.

Acknowledgment. We are indebted to Professor R. A. Jacobson for his assistance and for providing the equipment for the X-ray diffraction. It was also helpful to have the manuscript of Cotton and Zhong[8] prior to its publication. Support of this study by the NSF Grant CHE80-007442 is gratefully acknowledged.

Appendix

Davydov States for β- and γ-Tetrakis(μ-pivalato)dimolybdenum(II). The monoclinic, $I2/c$, structure possesses two crystallographically equivalent molecules in a primative cell. $\Phi_1'(k)$ and $\Phi_2'(k)$ designate Frenkel exciton bands for the two symmetry-equivalent molecular transitions for the excitation of a site 1 and a site 2 molecule, respectively, where k is the wave vector. The two Davydov bands may be represented by

$$\Phi_1'(k) = [\Phi_1'(k) + \Phi_2'(k)]/\sqrt{2} \quad (2)$$

$$\Phi_{II}'(k) = [\Phi_1'(k) - \Phi_2'(k)]/\sqrt{2} \quad (3)$$

Transitions are allowed only to the two Davydov states, $\Phi_1'(0)$ and $\Phi_{II}'(0)$. If the transition moment operators for the two symmetry-related molecules are μ_1 and μ_2, the transition moment vectors are given by $\mu_1 = \langle\Phi_1'|\mu_2|\Phi_1^0\rangle$ and $\mu_2 = \langle\Phi_2'|\mu_2|\Phi_2^0\rangle$ where Φ^0 and Φ' are ground- and excited-state molecular wave functions. The transition moments from the ground state, Φ^0, to the Davydov states, $\Phi_1'(0)$ and $\Phi_{II}'(0)$, are given by

$$\mu_I = \langle\Phi_1'(0)|\mu_1 + \mu_2|\Phi^0\rangle = \sqrt{N/2}(\mu_1 + \mu_2) \quad (4)$$

$$\mu_{II} = \langle\Phi_{II}'(0)|\mu_1 = \mu_2|\Phi^0\rangle = \sqrt{N/2}(\mu_1 - \mu_2) \quad (5)$$

where N is the number of unit cells in the crystal and the N factor results from the normalization of the exciton wave function. Since μ_1 is a vector, it can be expressed as

$$\mu_1 = xa + yb + zc \quad (6)$$

The c-glide plane reflection that converts molecule 1 into molecule 2 converts μ_1 into μ_2, so

$$\mu_2 = xa - yb + zc \quad (7)$$

Therefore

$$\mu_1 + \mu_2 = 2xa + 2zc \quad (8)$$

$$\mu_1 - \mu_2 = 2yb \quad (9)$$

One of the transition moments will lie along the b axis, and the other will be normal to the b axis.

The orthorhombic *Pbcn* crystal has four symmetry-equivalent molecules in a primative lattice cell. There are then transitions possible to four Davydov states with the wave vector, k, of 0.

$$\Phi_I'(0) = [\Phi_1'(0) + \Phi_2'(0) + \Phi_3'(0) + \Phi_4'(0)]/2 \quad (10)$$

$$\Phi_{II}'(0) = [\Phi_1'(0) + \Phi_2'(0) - \Phi_3'(0) - \Phi_4'(0)]/2 \quad (11)$$

$$\Phi_{III}'(0) = [\Phi_1'(0) - \Phi_2'(0) + \Phi_3'(0) - \Phi_4'(0)]/2 \quad (12)$$

$$\Phi_{IV}'(0) = [\Phi_1'(0) - \Phi_2'(0) - \Phi_3'(0) + \Phi_4'(0)]/2 \quad (13)$$

For *Pbcn* the four symmetry-related molecular transition moment vectors have the form

$$\mu_1 = xa + yb + zc \quad (14)$$

$$\mu_2 = -xa - yb + zc \quad (15)$$

$$\mu_3 = xa - yc - zc \quad (16)$$

$$\mu_4 = -xa + yb - zc \quad (17)$$

$$\mu_I = \langle\Phi_1'(0)|\mu_1 + \mu_2 + \mu_3 + \mu_4|\Phi^0\rangle = (N/2)(\mu_1 + \mu_2 + \mu_3 + \mu_4) = 0 \quad (18)$$

$$\mu_{II} = \langle\Phi_{II}'(0)|\mu_1 + \mu_2 + \mu_3 + \mu_4|\Phi^0\rangle = (N/2)(\mu_1 + \mu_2 - \mu_3 - \mu_4) = 2Nzc \quad (19)$$

$$\mu_{III} = \langle\Phi_{III}'(0)|\mu_1 + \mu_2 + \mu_3 + \mu_4|\Phi^0\rangle = (N/2)(\mu_1 - \mu_2 + \mu_3 - \mu_4) = 2Nxa \quad (20)$$

$$\mu_{IV} = \langle\Phi_{IV}'(0)|\mu_1 + \mu_2 + \mu_3 + \mu_4|\Phi^0\rangle = (N/2)(\mu_1 - \mu_2 - \mu_3 + \mu_4) = 2Nyb \quad (21)$$

Hence, a transition to state $\Phi_1'(0)$ is forbidden and three separate transitions will be aligned with the orthogonal a, b, and c axes, respectively.

Supplementary Material Available: Tables of anisotropic and isotropic thermal parameters (2 pages); tables of observed and calculated structure factors (11 pages). Ordering information is given on any current masthead page.

Contribution from the Department of Chemistry
and Molecular Structure Center, Indiana University, Bloomington, Indiana 47405

Alcohol Elimination Chemistry of $(CuO^tBu)_4$

T. H. Lemmen, G. V. Goeden, J. C. Huffman, R. L. Geerts, and K. G. Caulton*

Received January 18, 1990

The Bronsted basicity of $(CuO^tBu)_4$ was tested against a range of weak acids. With $(Ph_2P)_2CH_2$, ^tBuOH is eliminated, with production of the cage molecule $Cu_3(Ph_2PCHPPh_2)_3$, which was characterized by ^1H and ^{31}P NMR spectra. With Ph_2PH, ^tBuOH is eliminated to precipitate $(CuPPh_2)_x$, which can be dissolved with L = Ph_2PH or PPh_3 to give $[(Ph_2PH)CuPPh_2]_x$ and monomeric $Ph_3PCuPPh_2$. With $Ph_2P(CH_2)_2PPh_2$, deprotonation of a CH_2 group is followed by P-C bond cleavage to give $LCuPPh_2$, where L may be either $Ph_2PCH{=}CH_2$ or excess phosphine chelate. The vinyl group in this phosphine (either generated from $Ph_2P(CH_2)_2PPh_2$ or as added Ph_2PCHCH_2) is catalytically hydrogenated in this reaction system (100 atm H_2, 25 °C). $(CuO^tBu)_4$ reacts with PPh_3 to yield the dimer $(Ph_3PCuO^tBu)_2$, shown by X-ray diffraction to be a gull-winged dimer. This molecule does not dissolve intact in toluene, but shows partial phosphine ligand redistribution to $(CuO^tBu)_4$ and a more phosphine-rich species. Crystallographic data (−165 °C): a = 10.327 (4) Å, c = 36.669 (20) Å with Z = 4 in space group $P4_12_12$.

Introduction

We recently reported several cases[1,2] in which $(CuO^tBu)_4$ reacts with transition-metal hydride complexes to couple the two metals with simultaneous elimination of alcohol (eqs 1 and 2; P = PMe_2Ph). Such a bimolecular reductive elimination is particularly interesting since it gives the appearance of proton transfer to basic alkoxide oxygen, yet an X-ray crystallographic study[3] of the copper reagent I has shown it to contain three-coordinate oxygen. Such a μ_2-alkoxide oxygen would appear to be, at best, a weak base.

$$\tfrac{1}{4}(CuO^tBu)_4 + H_4OsP_3 \rightarrow \tfrac{1}{3}(H_3CuOsP_3)_3 + {}^tBuOH \quad (1)$$

$$\tfrac{1}{2}(CuO^tBu)_4 + 2Re_2H_8P_4 \rightarrow Cu_2Re_4H_{14}P_8 + 2{}^tBuOH \quad (2)$$

Part of the reason for suggesting a proton-transfer mechanism for eqs 1 and 2 rests on the work of Saegusa et al.,[4] who reported that $(CuO^tBu)_4$ reacts with carbon acids to form ^tBuOH and a Cu-C bond (eqs 3 and 4). Additional evidence for basicity at

(1) Lemmen, T. H.; Huffman, J. C.; Caulton, K. G. *Angew. Chem., Intl. Ed. Engl.* **1986**, *25*, 262.
(2) Sutherland, B. R.; Ho, D. M.; Huffman, J. C.; Caulton, K. G. *Angew. Chem., Intl. Ed. Engl.* **1987**, *26*, 135.
(3) Greiser, T.; Weiss, E. *Chem. Ber.* **1976**, *109*, 3142.
(4) Tsuda, T.; Hashimoto, T.; Saegusa, T. *J. Am. Chem. Soc.* **1972**, *94*, 658.

0020-1669/90/1329-3680$02.50/0